Investigating Gas Diffusion Electrode Flooding in CO_2 Electrolysis With an Operando Water Trap System: The Role of (Bi)carbonate Salt Precipitation

[z]Daniel Rottmann[1,2], Ricarda Kollmuss[1], Stefan Haufe[1], Urban Sajevic[3], Karl J. J. Mayrhofer[2,3]

Affiliations:
[1]Wacker Chemie AG, Consortium für elektrochemische Industrie, Zielstattstr. 20, 81379 Munich, Germany
[2]Department of Chemical and Biological Engineering, Friedrich-Alexander University Erlangen-Nürnberg, Cauerst. 1, 91058, Erlangen, Germany
[3]Helmholtz Institute Erlangen-Nürnberg for RenewableEnergy (IEK-11), Forschungszentrum Jülich GmbH, Cauerst. 1, 91058 Erlangen (Germany)

[z]Corresponding Author E-mail Address: daniel.rottmann@wacker.com

Abstract

The electrochemical reduction of CO_2 (CO_2 electrolysis) is a promising technology for not only reducing CO_2 emissions, but also contributing to a circular carbon economy. However, industrial feasibility has not been achieved yet, as flooding of the gas diffusion electrode (GDE) limits the long-term stability of CO_2 electrolysis. Although (bi)carbonate salt precipitation is often considered to be one of the main factors accelerating GDE flooding, direct evidence of this effect is still lacking and further investigations are needed. In this study, we address this gap by employing an operando water trap to quantify GDE flooding in a time-resolved manner. The results demonstrate a direct correlation between salt precipitation and GDE flooding, as (bi)carbonate catholytes show increased GDE flooding rates. Additionally, the bicarbonate anion (HCO_3^-) was identified as the harmful species, independent of the catholyte's pH. However, GDE flooding still occurs even when bicarbonate formation is mitigated, albeit at a much slower rate, indicating the need to investigate additional contributing factors.

Introduction

Climate change, caused by greenhouse gas emissions such as CO_2, is one of the most urgent challenges humanity is facing today[1, 2]. In this regard, using CO_2 as a feedstock for the chemical industry has become of major interest to reduce CO_2 emissions and create a circular carbon economy[3, 4]. The electrochemical reduction of CO_2 is a promising technology using intermittent renewable electricity (e.g. from solar or wind) to convert CO_2 emissions into valuable platform chemicals such as ethylene, carbon monoxide or methane. However, up to this day industrial feasibility of the process has not yet been reached[5, 6].

To achieve industrially relevant current densities (> 100 mA cm^{-2} [7, 8]), CO_2 electrolyzers often use gas diffusion electrodes (GDEs), which enable a high CO_2 mass transport to the catalyst[9]. These GDEs consist of a porous gas diffusion layer (GDL) with a microporous layer (MPL) and a catalyst layer (CL) on top. The GDL enables efficient CO_2 transport to the CL by maintaining a triple phase boundary at the catalyst/electrolyte/gas interface, creating a short diffusion path for CO_2 to the catalyst´s active sites[9, 10]. Nevertheless, especially when reaching industrially relevant current densities, the liquid electrolyte floods the GDE pores within a short period of time[11, 12]. This flooding shifts the position of the gas-liquid interface away from the catalyst, resulting in a longer diffusion path for CO_2 to the catalyst and therefore mass transport limitation. As a consequence, a shift from the electrochemical CO_2 reduction to the hydrogen evolution reaction (HER) is observed[10]. This fast decay in CO_2 conversion remains one of the main technical challenges, as long-term operation stability of 60,000-90,000 h is needed for industrial feasibility[13]. Addressing the issue of GDE flooding is therefore critical to reach industrial relevance.

To this day, the reasons for GDE flooding are intensively discussed within the literature and multiple explanations for this phenomenon have been proposed, such as electrowetting[14–17], salt precipitation within the GDE[18–24], uneven pressure distribution at the GDE/electrolyte interface[25], degradation of polytetrafluoroethylene (PTFE) within the GDE [15] and surface tension reduction due to liquid product formation[26]. While the individual contributions of each possible reason to the observed GDE performance degradation is dependent on multiple parameters such as cell design[22, 27, 28] or electrolyte pH[21, 29, 30], especially salt precipitation through the GDE has often been described as a major contributor to GDE flooding. This process occurs during electrolysis, where electro-generated OH^- ions or OH^- ions from the electrolyte react with dissolved CO_2 molecules to produce carbonate and bicarbonate anions (see Equation 1 and 2)[20].

$$\boldsymbol{CO_2(aq) + OH^-(aq) \rightleftharpoons HCO_3^-(aq)} \quad (1)$$

$$\boldsymbol{HCO_3^-(aq) + OH^-(aq) \rightleftharpoons CO_3^{2-}(aq) + H_2O(l)} \quad (2)$$

At steady state, both (bi)carbonate anions and alkali metal cations from the electrochemical double layer are present in excess of the solubility limit, which leads to carbonate salt precipitation within the GDE[19]. These carbonate salt precipitates are believed to facilitate GDE flooding due to their hygroscopic nature, however, direct evidence of this effect is absent [31].

The aim of this work is to contribute to a better understanding of (bi)carbonate salt precipitation and its influence on GDE flooding during CO_2 electrolysis. A new perspective on this failure mechanism is achieved by using our previously published operando water trap system (also referred to as in-operando water trap[32]), which simultaneously quantifies GDE flooding, while a gas chromatograph (GC) simultaneously determines the gaseous product distribution [32]. The results indicate that salt precipitation is a major contributor to GDE flooding within flow cell electrolyzers during CO_2 electrolysis. However, salt precipitation is not the sole contributor to GDE flooding. During CO electrolysis where carbonation of the electrolyte does not happen, flooding is also observed, albeit at much lower rate. Despite comparably slower flooding the CO electrolysis showed a faster increase in HER. This may be attributed to the lower solubility of CO compared to CO_2 in aqueous electrolytes[33].

Experimental

GDE preparation: The GDE cathode was prepared by coating a 13.5 x 13.5 cm^2 gas diffusion layer (Freudenberg, H23C8) with a catalyst ink containing Cu nanoparticles (Sigma-Aldrich, 40-60 nm) and Nafion™ (Ion Power, 20 wt.%) in an 88:12 mass ratio. The ink was prepared with a 1.0 wt.% solids content by dispersing the Cu nanoparticles and Nafion™ in a 50:50 vol.% isopropanol/water mixture using an ultrasonic horn (Hielscher, UIS250v) for 30 min while the mixture was continuously cooled in an ice bath. Afterwards, the catalyst ink was coated onto the GDL using a home-built inkjet printing system. The inkjet printer consisted of an inkjet spray head (Vermes, MDS1560 equipped with a ceramic pestle CTF 4) connected to an xyz-plotter (imes-icore, ICV 4030 xyz). The catalyst ink was continuously recirculated through the spray head by a micro gear pump at 350 ml min^{-1} to avoid ink sedimentation during the printing process. In addition, the catalyst ink was kept under 0.2 bar nitrogen pressure to prevent unwanted Cu oxidation and to keep the hydrostatic pressure constant. The GDL was placed on a heated aluminum plate, temperature-controlled to 90 °C, underneath the printing unit. The printhead moved in serpentines over the GDL surface, while small ink droplets were propelled at 41 Hz from the nozzle onto the GDL, where the solvent evaporated immediately. The final mass loading was controlled by the number of printing runs on the GDL.

Electrolysis setup: A Micro Flow Cell® (ElectroCell) was used for all CO_2 electrolysis experiments. The cell consisted of a gas compartment, a catholyte compartment and an anolyte

compartment. Catholyte and anolyte were separated by a bipolar membrane (Fumasep® FBM, FUMATECH BWT, geometric area 10 cm^2), whereas the gas compartment and catholyte compartment were separated by the cathode/GDE (geometric area 5 cm^2). For the anode an Ir-MMO plate (ElectroCell, geometric area 10 cm^2) was used. The potentials of the working and counter electrodes were monitored against an Hg/HgO reference electrode (BioLogic), located in the catholyte at the cell entrance.

Both the catholyte and the anolyte consisted of 220 ml 1 M KOH prepared with KOH pellets (Sigma-Aldrich, ACS reagent) and ultrapure water (Arium® mini, Sartorius, 18.2 MΩ cm), which were recirculated through the cell using micro gear pumps. The catholyte was recirculated at 5 ml min^{-1} and the anolyte at 33 ml min^{-1}. The CO_2 (Linde, purity 2.5) volume flow was controlled by a mass flow controller (Bronkhorst, El-Flow select) and was held constant at 40 ml min^{-1}. The complete setup is depicted in Figure S1.

Electrochemical procedure: The electrolysis cell was operated galvanostatically by a potentiostat (BioLogic, SP150-E + 20 A booster). Before each experiment, the cell was equilibrated for 4 min at open circuit voltage (OCV) while CO_2 gas and electrolytes were flowing. The current density was then increased to the setpoint for chronopotentiometry using linear sweep amperometry (LSA) with a ramp of 2 mA s^{-1} cm^{-2}. After reaching the desired current density, chronopotentiometry was applied and the quantification of the gas products and the percolation rate was started.

Quantification of CO_2 electrolysis products and leakage: Gas chromatography was employed to quantify the gaseous products and their respective gas volume flow rates ($\dot{V}_{prod}$). A gas chromatograph (8860, Agilent, modified by Joint Analytical Systems GmbH) equipped with a thermal conductivity detector was used for the quantification of the concentrations and the gas flow of the gaseous products. Using Helium (Linde, quality 5.0) as a carrier gas and three serially connected columns (Hayesep Q, HP-PLOT-Q, HP-PLOT 5A), an automated injection, separation and quantification of the product gas stream was possible every 9.5 min.

The product gas flow ($\dot{V}_{prod}$) was determined by dosing an additional N_2 volume flow ($\dot{V}_{N2}$, 20 ml min^{-1}) into the product gas stream shortly before the GC. This N_2 volume flow acted as an internal standard and allowed to determine $\dot{V}_{prod}$ according to the following equation:

$$\dot{\boldsymbol{V}}_{\boldsymbol{prod}} = \frac{\dot{\boldsymbol{V}}_{\boldsymbol{N2}}}{\boldsymbol{\varphi}_{\boldsymbol{N2}}} - \dot{\boldsymbol{V}}_{\boldsymbol{N2}} \tag{3}$$

with φ_{N2} being the volume fraction of N_2 within the product gas flow. It should be noted that the GC was calibrated with N_2/Ar gas mixtures between 1-100 vol. % to ensure correct N_2 quantification. These mixtures were prepared using two mass flow controllers (Bronkhorst, El-Flow select), which were prior calibrated with a DryCal flow meter (Mesalabs, FlexCal).

The GC calibration for the CO_2 electrolysis products was accomplished by injecting calibration gases (Tyczka) including the following components: CH_4, C_2H_6, C_2H_4, CO, H_2 and CO_2. The different calibration points were obtained by diluting the initial calibration gas. The Faradaic efficiencies (FE) of the individual gaseous products were determined using the following equation:

$$\boldsymbol{FE_i = \frac{\varphi_i \times \dot{V}_{prod} \times F \times z_i}{V_M \times I} \times 100\,\%} \tag{4}$$

with F being the Faraday constant (96.485 $\frac{C}{mol}$), z the stochiometric number of electrons consumed for the individual product (CH_4 = 8, C_2H_6 = 14, C_2H_4 = 12, CO = 2 and H_2 = 2), V_M the molar volume of an ideal gas (22.41 $\frac{l}{mol}$), I the applied current and φ_i the volume fraction inside the product gas stream of the individual products. It should be mentioned that the dilution by the internal N_2 standard must be taken into account when calculating the volume fractions of the product gases quantified with the GC ($\varphi_{i,N2\,diluted}$). A conversion was carried out according to Equation (5):

$$\boldsymbol{\varphi_i = \frac{\varphi_{i,N2\,diluted} \times (\dot{V}_{prod} + \dot{V}_{N2})}{\dot{V}_{N2}}} \tag{5}$$

At the end of an experiment, Nuclear magnetic resonance (NMR) spectroscopy was used to quantify liquid CO2RR products (ethanol, propanol, acetic acid, formic acid) within the catholyte. Measurements were conducted with an Avance III HD 500 MHz (Bruker) NMR spectrometer equipped with a SampleXpress autosampler. Each catholyte sample was measured twice with two different internal standards. Liquid products upfield of the water signal were referenced to sodium trimethylsilylpropanesulfonate (DSS) as internal standard, while peaks downfield of the water signal were referenced to potassium hydrogen phthalate (KHP) as internal standard. In detail 540 µl of catholyte was taken after the experiment and mixed with 60 µl internal standard (either 0.1 mg ml^{-1} DSS or 1.0 mg ml^{-1} KHP solved in D_2O) to have an overall sample volume of 600 µl. The samples were measured with the water suppression pulse sequence noesygppr1d (1D NOESY with pre-saturation and spoil gradients) to suppress the water peak and facilitate evaluation. One experiment consisted of 64 scans with

a delay time (d1) of 60 seconds to ensure quantitative relaxation of all relevant nuclei.

Quantification of electrolyte leakage through the GDE during electrolysis was performed using an analytical tuning fork balance (Kern & Sohn, PNS3000-2). Electrolyte droplets formed on the backside of the GDE are being pulled by gravitational force and gas flow towards the water trap. The water trap is positioned below and slightly offset of the electrolyzer cell, which allows electrolyte droplets to move via gravitational force towards the water trap. It is connected to the cathode's gas outlet via flexible tubing (PROLIQUID, TYGON A-60-C). The analytical balance measured the amount of percolated electrolyte during chronopotentiometry. This allows to calculate percolation rates over the experiment's course:

$$\boldsymbol{Leakage\ rate} = \frac{\boldsymbol{\Delta m}}{\boldsymbol{t} \times \boldsymbol{A}} \tag{6}$$

with Δm being the collected mass of electrolyte [mg] during the time period, t the length of the period [min] and A being the geometric area of the working electrode. The leakage rate is calculated for each individual time segment (e.g., 30-60 min or 60-90 min), not cumulatively from the beginning of the experiment.

Results and Discussion

The accumulation of (bi)carbonate anions during CO_2 electrolysis leads to salt precipitation within the GDE[18, 20]. To better understand this process and the potential impact of salt precipitation on GDE flooding, leakage rates and gaseous product distributions were measured during CO_2 electrolysis in 1 M KOH. Additionally, the pH of the catholyte was measured at different points in time (see SI) to monitor the formation of (bi)carbonate anions. The 1 M KOH electrolyte was continuously neutralized by the CO_2 gas stream to 0.5 M K_2CO_3 and finally to 1 M $KHCO_3$. At an alkaline pH between 11 to 14, the dissolved CO_2 is predominantly converted to carbonate (CO_3^{2-}) anions. In contrast, the carbonate equilibrium shifts towards the bicarbonate (HCO_3^-) anion at a pH of 7 to 10 [34].

Electrochemical CO_2 reduction is performed under industrially relevant current densities of 200 mA cm^{-2} using 1 M KOH as catholyte and anolyte. Gaseous product distributions are determined every 9.5 min, while leaked electrolyte is quantified every minute. Average leakage rates are calculated over 30 min intervals (see Equation 6). The pH of the catholyte was determined at the beginning of the experiment as well as after 3 and 7 hours of operation. Figure 1shows the time-resolved FEs of the gaseous products from the CO2RR, given by the

sum of FE_{CO} (40-50 % initially) and FE_{C2H4} (10-15 % initially) amounting to roughly 60 % in total in the beginning, along with the FE_{H2} and leakage rates. Note that the formation of liquid products is not included in the time-resolved representation of the FEs, since our NMR method for liquid product quantification can only determine an average FE for the liquid products over the entire experiment duration (see Figure S2).

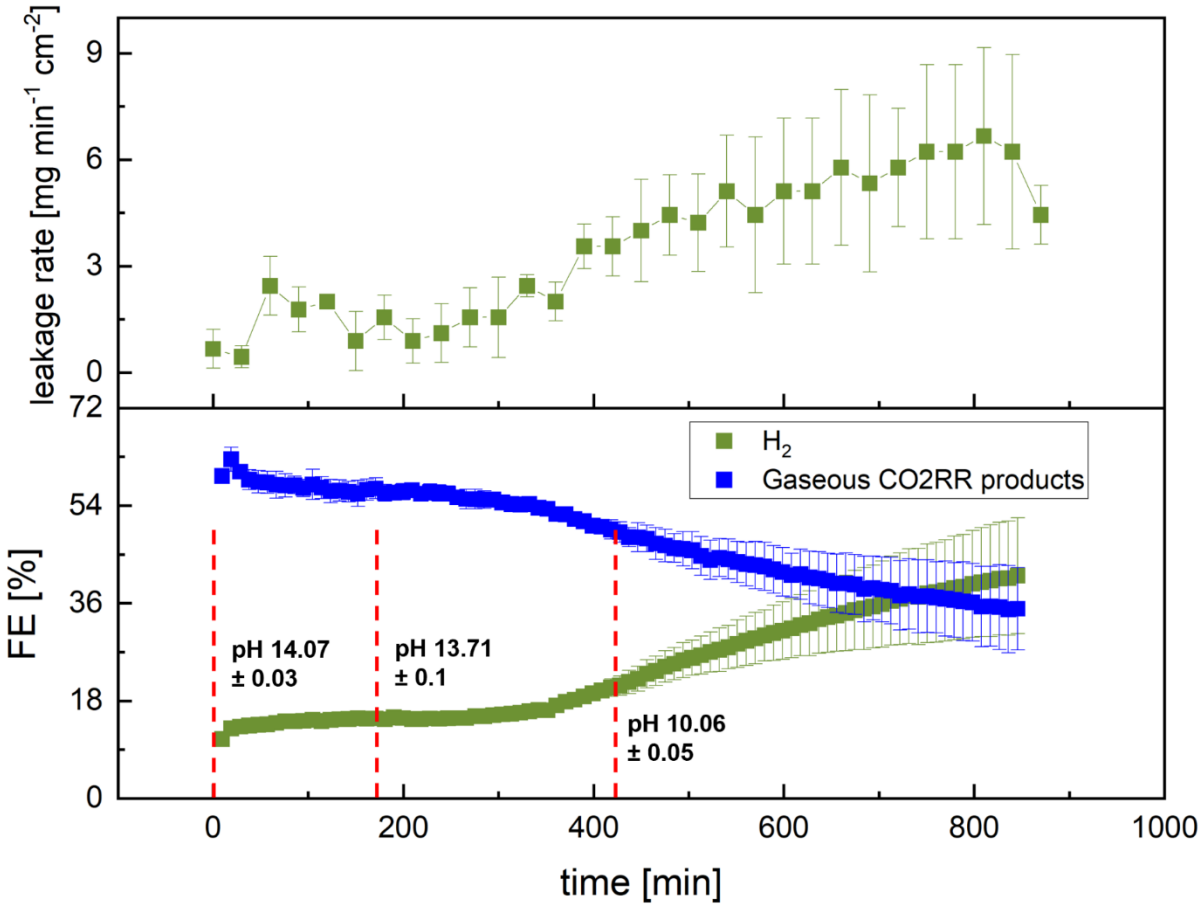

Figure 1 Temporal progression of FEs of gaseous CO2RR products (C_2H_4 and CO) and H_2 along with the leakage rates, in 1M KOH under galvanostatic conditions at 200 mA cm^{-2}. The pH of the catholyte was determined at the beginning as well as after 3 and 7 hours of operation. Each pH value shown is calculated from two measurements. The error bars represent the standard deviation of three independent experiments. GDE leakage and HER increase as soon as the HCO_3^- dominant regime (around pH 10) is reached. This could indicate that $KHCO_3$ salt precipitation in particular leads to flooding of the GDE.

Figure 1 shows that after 3 h of electrolysis the pH level is still highly alkaline (around pH 13.7). At this pH, the predominant carbonate species in the electrolyte is carbonate (CO_3^{2-}) anion. In contrast, after 7 h of operation the pH is around 10 and the main carbonate species is

the bicarbonate (HCO_3^-) anion. Comparing these results with the leakage rates indicate that the shift towards the HCO_3^- species apparently leads to increased flooding. Between 0-390 min when the pH is still alkaline and CO_3^{2-} is the dominant species, the leakage rates are constant at 1.8 mg min^{-1} cm^{-2}. However, a continuous increase in the leakage rates of up to 4 mg min^{-1} cm^{-2} is observed after ca. 400 min. A similar trend can be seen for the FEs of the gaseous CO2RR products and H_2. Up to about 390 min, a steady formation of the gaseous CO2RR products and H_2 can be observed. Afterwards and at the same time when the leakage rates start to increase, a continuous shift from CO2RR to HER can be observed. This indicates that after ca. 400 min GDE flooding increases and consequently mass transport limitation favors HER. As mentioned before, liquid product formation could not be monitored in a time-resolved manner here. Nevertheless, a similar trend for the liquid product formation is to be expected as flooding induced mass transport limitations reduce CO_2 availability and consequently shift the reaction from the CO2RR to the HER[10]. This was also reported by Zhu *et al.* who used their inline operando NMR method to monitor the time-resolved formation of liquid products. A decrease in liquid product formation was observed when salt precipitation became more pronounced[35].

Results from Figure 1 suggest that the formation of bicarbonate (HCO_3^-) and thus the precipitation of $KHCO_3$ salt within the GDE accelerates flooding. To investigate this hypothesis, the precipitated salts on the CL after 4 and 7 h of operation were analyzed by IR spectroscopy (see SI). After 4 hours operation, the pH remains strongly alkaline (pH 13.5), with CO_3^{2-} as the dominant species, and thus K_2CO_3 is expected as the precipitated salt. In contrast, after 7 hours (pH 10) the formation of $KHCO_3$ as a precipitate is expected. Figure 2 shows the IR spectra of the salt crystals analyzed after different times of operation. The IR spectra of K_2CO_3 and $KHCO_3$ are shown in the supporting information (Figure S3).

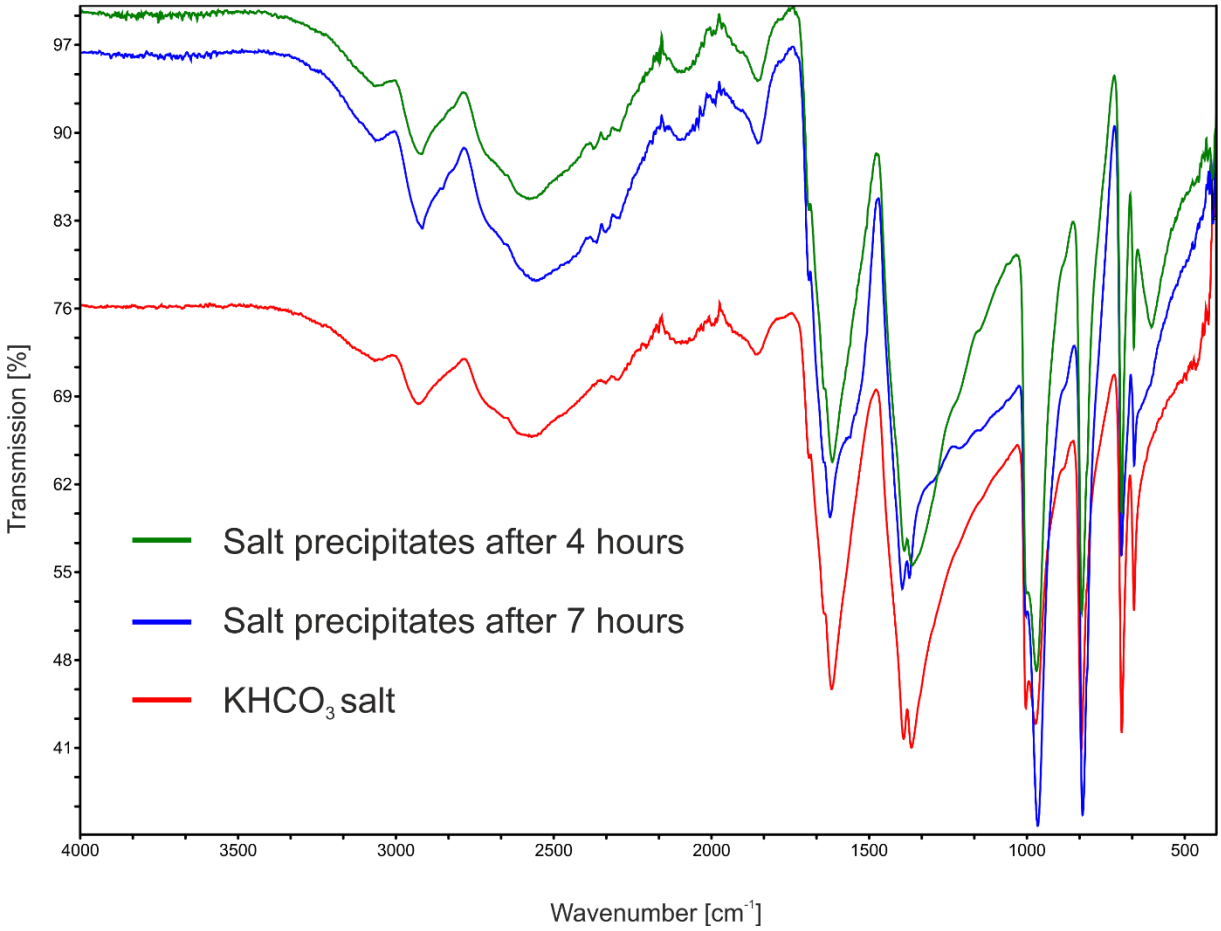

Figure 2 IR spectra of salt crystals formed on the CL after 4 and 7 h of CO_2 electrolysis. Both spectra indicate the formation of $KHCO_3$, which could be due to the comparatively low solubility of $KCHO_3$.

The IR spectra after 4 and 7 h of electrolysis confirm the formation of $KHCO_3$ salt on the CL. However, the precipitation of $KHCO_3$ in the strongly alkaline pH value within 4 hours was not expected. $KHCO_3$ has a comparably lower solubility in H_2O (3.62 mol kg^{-1} H_2O) than K_2CO_3 (8.03 mol kg^{-1} H_2O) or KOH (21.57 mol kg^{-1} H_2O), which could explain why $KHCO_3$ precipitates more easily in the GDE even at high pH values[36]. This hypothesis is supported by results from Cofell *et al.* who observed a higher resistance to salt precipitation and GDE flooding when switching from KOH to CsOH, due to the higher solubility of $CsHCO_3$ in comparison to $KHCO_3$ in H_2O [21].The formation of $KHCO_3$ in the CL throughout different pH levels in combination with the increase in leakage rates at the HCO_3^- dominant pH regime indicates that the precipitation of $KHCO_3$ salt increases GDE flooding. Similar observations were made by Leonard *et al.* who were able to recover their GDE performance after electrolysis by cleansing their GDE from salt precipitates. [36]. This further suggests that salt precipitation within the GDE acts as a promoter for flooding. Note that the extent of performance recovery

depended on the employed salt-removal procedure and deeply embedded salt crystals were difficult to remove.

Based on the results from Figure 1 and 2 the GDE flooding behavior during CO_2 electrolysis was investigated depending on the electrolyte using 0.5 M K_2CO_3 and 1 M $KHCO_3$. As previously mentioned, 1 M KOH is continuously neutralized by CO_2 from the gas stream (see Figure 1), initially forming 0.5 M K_2CO_3 and finally 1 M $KHCO_3$. These experiments therefore represent different stages of 1 M KOH neutralization and consequently investigate the influence of (bi)carbonate salt precipitation on GDE flooding.

In these experiments, CO_2 electrolysis was also carried out at a current density of 200 mA cm^{-2}. Figure 3 shows the time-resolved FEs of gaseous products from the CO2RR (C_2H_4 and CO) and H_2, along with the leakage rates. For comparison purposes, the results in 1 M KOH (Figure 1) are also depicted.

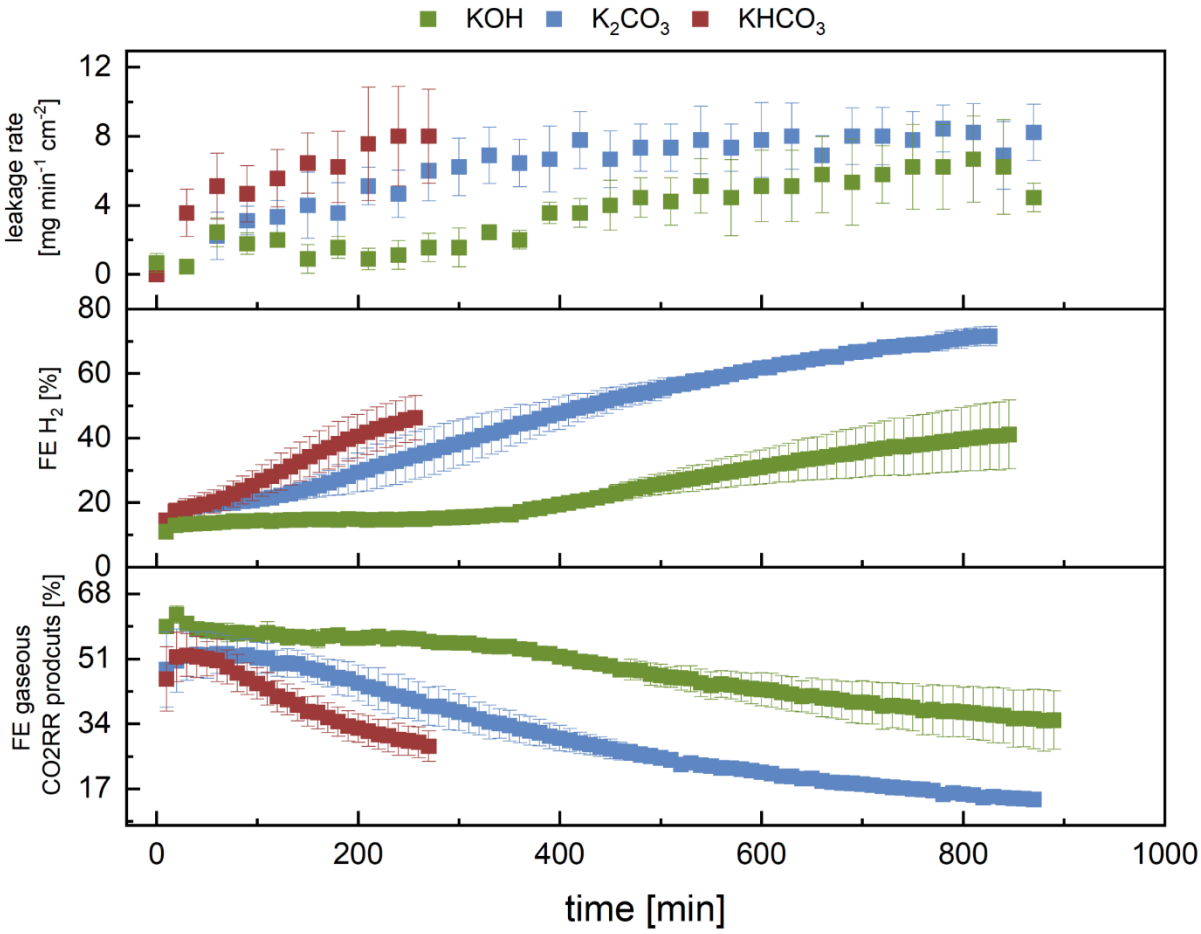

Figure 3 Temporal progression of FEs at a current density of 200 mA cm^{-2} of gaseous CO2RR products (CO and C_2H_4) and H_2 along with leakage rates in 1 M KOH, 0.5 M K_2CO_3 and 1 M $KHCO_3$, respectively. Experiments in 0.5 M K_2CO_3 and 1 M $KHCO_3$ represent different

stages of 1 M KOH neutralization by CO_2. The error bars show the standard deviation of three experiments each. Leakage rates and gaseous product FEs indicate that GDE flooding is enhanced by the precipitation of (bi)carbonate salt.

The results from Figure 3 show that the leakage rates of the three electrolytes differ significantly over time. For 1 M KOH, the leakage rates remain steady at approximately 1.8 mg min^{-1} cm^{-2} during the first 390 min. However, after ca. 400 min, the leakage rates start to increase, eventually reaching a maximum rate of approximately 6 mg $min^{-1}cm^{-2}$. In contrast, the 0.5 M K_2CO_3 and 1 M $KHCO_3$ electrolytes exhibit increasing leakage rates from the beginning and reach a similar maximum value to 1 M KOH after only about 270 min (0.5 M K_2CO_3) and 150 minutes (1 M $KHCO_3$). When comparing the FEs for gaseous CO2RR products (CO and C_2H_4) and H_2, it is found that the carbonate-based electrolytes (0.5 M K_2CO_3 and 1 M $KHCO_3$) show a much faster shift from CO2RR to the HER compared to 1 M KOH. The higher stability of CO2RR observed with 1 M KOH is likely due to its comparatively lower leakage rates, indicating a slower flooding process. These results further support that the accumulation of (bi)carbonate species in the catholyte and the resulting salt precipitation accelerate the flooding of the GDE. Additionally, the experiments with 0.5 M K_2CO_3 and 1 M $KHCO_3$ confirm that the shift towards the HER in 1 M KOH primarily arises from progressive GDE flooding rather than from a continuous decrease of the catholyte's pH (see Figure 1). If pH drift would be the dominant factor, differences in FE_{H2} would be visible from the beginning, due to the lower pH levels of 0.5 M K_2CO_3 and 1 M $KHCO_3$ in comparison to 1 M KOH. However, 0.5 M K_2CO_3 (FE_{H2} 16 %) and 1 M $KHCO_3$ (FE_{H2} 17 %) show similar initial FE_{H2} as 1 M KOH (FE_{H2} 13 %), confirming GDE flooding as the main contributor for the shift towards the HER.

Comparing 0.5 M K_2CO_3 and 1 M $KHCO_3$, 1 M $KHCO_3$ shows a faster shift from CO2RR to HER over time. This is consistent with the leakage rate trends, as a more rapid increase in leakage can be observed when using 1 M $KHCO_3$. Additionally, only 1 M $KHCO_3$ shows notable leakage within the first 30 min, further supporting the hypothesis that mainly $KHCO_3$ salt precipitates in the GDE due to its lower solubility and accelerates flooding. It should be noted, that the leakage rates appear to reach a state of equilibrium at some point, while the HER increases continuously. This could indicate that the GDE flooding has reached a maximum value, but other failure mechanism such as pore blocking or catalyst degradation are increasing HER further[19, 37, 38].

Since the results from Figure 1-3 strongly indicate that the precipitation of bicarbonate salts leads to increased flooding of the GDE, the stability of the GDE was subsequently investigated without salt precipitation. This was accomplished by switching from CO_2 to CO electrolysis. CO does not react with OH^- anions to form (bi)carbonate[39–41], so no precipitation of bicarbonate salt takes place during CO electrolysis, as additionally confirmed by IR measurement (see Figure S4).

In detail, CO electrolysis was performed in 1 M KOH under galvanostatic conditions at 200 mA cm^{-2}. For better comparison, results from Figure 1 for CO_2 electrolysis in 1 M KOH at 200 mA cm^{-2} are also shown.

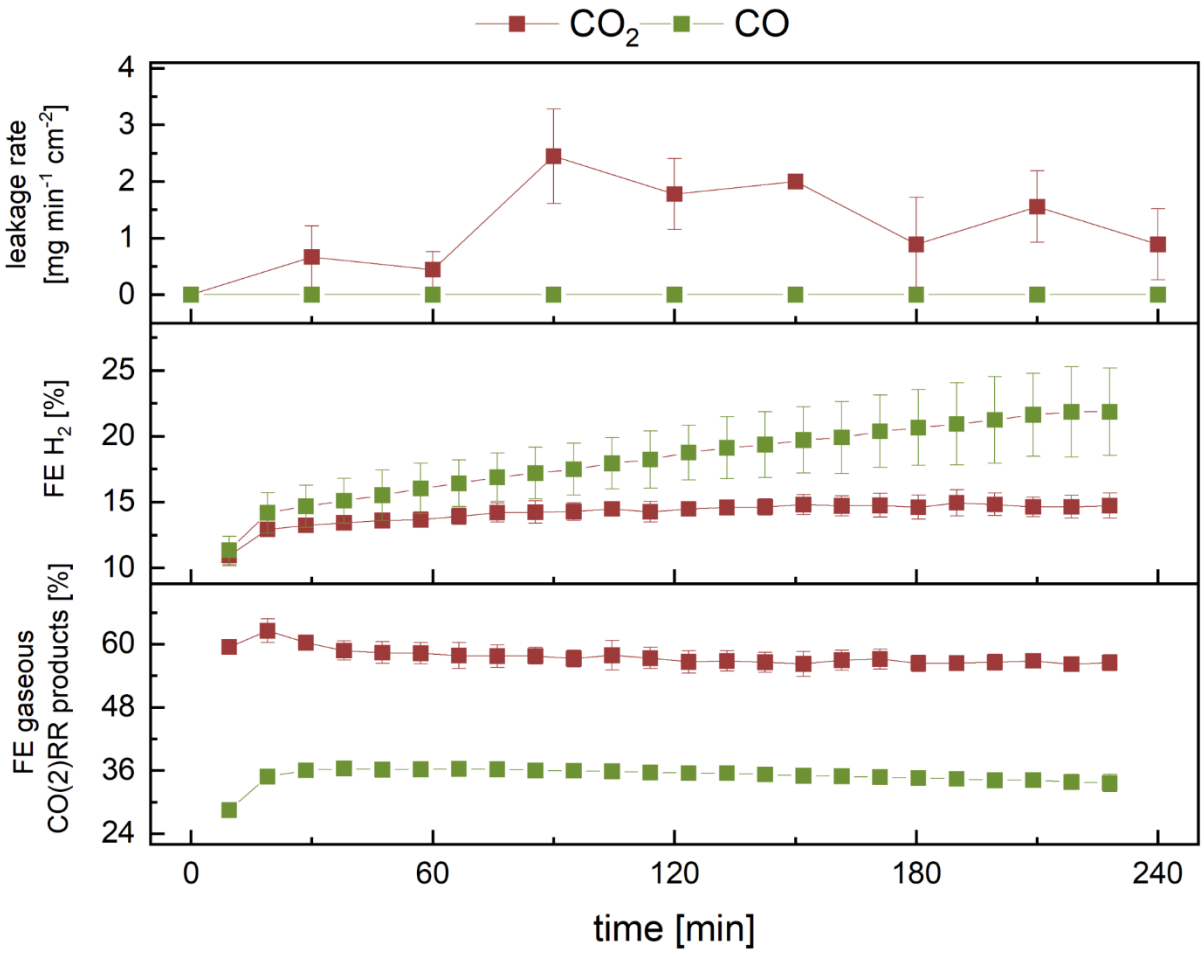

Figure 4 Temporal progression of FEs at a current density of 200 mA cm^{-2} of gaseous CO(2)RR products and H_2 along with leakage rates in 1 M KOH. The error bars represent the standard deviation of three experiments each. No leakage was observed during CO electrolysis,

which indicates that GDE flooding was at least strongly suppressed. Despite the strongly suppressed leakage, a rapid increase in HER is observed.

The results from Figure 3 show that there was no electrolyte leakage from the GDE within 4 h during CO electrolysis. In contrast, electrolyte leakage already occurs within the first 30 min of CO_2 electrolysis. Since the leakage rate quantifies GDE flooding, this would mean that flooding of the GDE is at least strongly suppressed during CO electrolysis and perhaps only takes place much more slowly within the GDE. This observation further supports the hypothesis that bicarbonate salt precipitation enhances GDE flooding, as no (bi)carbonate anions are formed during CO electrolysis. When the leakage rates are compared with the FE_{H2} for CO and CO_2 electrolysis, it can be observed that CO electrolysis shows a faster increase in HER. This result was not expected, since lower leakage rates indicate slower GDE flooding and thus imply a slower increase in HER. A possible explanation could be the lower solubility of CO (0.99 mM) compared to CO_2 (34 mM) in water under standard conditions, which could lead to an earlier onset of mass transport limitation by GDE flooding[42]. Although GDE flooding is suppressed during CO electrolysis, it could lead to a faster limitation of mass transport due to the low solubility of CO in the aqueous electrolyte. While HER increases with time, the FE for the gaseous CORR product C_2H_4 stays constant. Since CO is an important intermediate towards C_2H_4, the formation of C_2H_4 depends on the CO* concentration at the CL[43]. The constant FE for C_2H_4 could therefore be explained by a sufficient CO* concentration maintained during CO electrolysis. suggesting that the FE towards the liquid products decreases over time, which is not monitored by the operando water trap system.

Determining whether the GDE was flooded exclusively inside the GDE during CO electrolysis is not possible with the operando water trap, as flooding is measured by the amount of electrolyte flowing through the GDE (leakage). To investigate whether flooding occurred within the GDE during CO electrolysis, the cross sections of the GDE was analyzed after operation (see SI) using scanning electron microscopy (SEM) and energy dispersive X-ray spectroscopy (EDX). These techniques allow to localize potassium residues inside the GDE after electrolysis and thus provide an indication of whether GDE flooding has taken place[20, 23]. If flooding of the GDE occurred during the CO electrolysis experiments, potassium residues should be found within the CL and/or GDL. Otherwise, potassium should only be found on top of the CL, as no penetration into the pores has taken place.

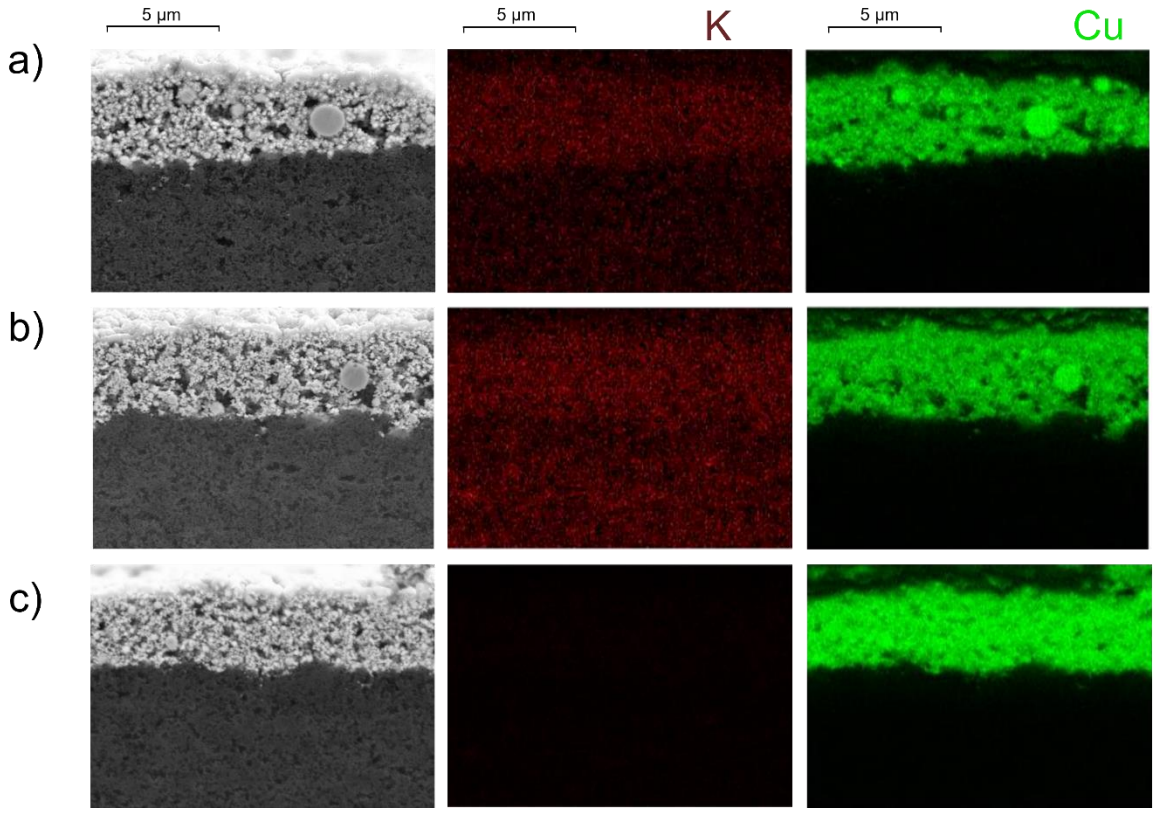

Figure 5 SEM and EDX of GDE cross-sections a) after 4h of CO electrolysis, b) after 4h of CO_2 electrolysis, c) before electrolysis. Potassium was detected in the CL and MPL after CO and CO_2 electrolysis, which indicates that flooding of the GDE has taken place in both cases.

Figure 5 shows the SEM/EDX cross-sections GDEs after 4 h of CO_2 and CO electrolysis. For comparison, the cross-section of a GDE before electrolysis is also shown. It can be observed that the unused GDE (Figure 5c) had no detectable potassium within the CL or MPL, indicating that the GDE was initially free of potassium. However, significant differences are observed after electrolysis. After 4 h of CO_2 electrolysis (Figure 5b) potassium was detected in both the CL and MPL, indicating that the GDE was flooded during the electrolysis process. This is consistent with Figure 4, in which the flooding of the GDE during CO_2 electrolysis was quantified with the operando water trap. In contrast, the GDE subjected to 4 h of CO electrolysis (Figure 4a) contains potassium within its CL and MPL, confirming that GDE was flooded during CO electrolysis. However, no leakage was detected during the CO electrolysis experiment (Figure 4). This indicates that although GDE flooding occurs during CO and CO2 electrolysis, the flooding rate is significantly lower during CO electrolysis. To investigate this hypothesis, the potassium content in the GDEs after CO and CO_2 electrolysis was quantified, since a higher degree of pore intrusion/GDE flooding leads to a higher potassium content after

electrolysis. Although EDX spectroscopy can be used for quantitative elemental analysis, only a small fraction of the GDEs is analyzed. Therefore, additional measurements with inductively coupled plasma optical emission spectroscopy (ICP-OES) measurements were performed to quantify the potassium content in the GDEs after 4 hours of CO and CO_2 electrolysis. The potassium content after 4 hours of CO_2 electrolysis (4.9 mg K inside the GDE) was more than twice as high as after 4 hours of CO electrolysis (2.2 mg K inside the GDE). These ICP-OES results confirm that flooding is slower during CO electrolysis in comparison to CO_2 electrolysis, which is consistent with the observed leakage rates from Figure 3.

The results from Figures 3 and 4 suggest that precipitation of bicarbonate salt contributes significantly to GDE flooding. However, since GDE flooding also occurs without bicarbonate formation during CO electrolysis, albeit at a slower rate, other factors must contribute to flooding during this process. As discussed earlier, several possible reasons for flooding of the GDE besides carbonate salt precipitation have been identified, e.g. electrowetting, formation of liquid, pressure fluctuations in the GDE and PTFE degradation. Although further investigation is needed to determine the main cause(s) of GDE flooding during CO electrolysis, we assume that liquid product formation is not a major contributor to GDE flooding. The rates of liquid product formation were 3 to 5 times higher for CO electrolysis than for CO_2 electrolysis, but CO_2 electrolysis had much higher leakage rates (see Figure S5). However, it should be noted that the influence of liquid products on GDE flooding may be more apparent after longer periods of time and consequently higher liquid product concentrations. PTFE degradation could contribute to flooding of the GDE during CO electrolysis. However, this phenomenon was observed on a special carbon-free GDE, not on a carbon-based GDE as used in our experiments[15]. The influence of non-uniform pressure distribution across the GDE and the electrowetting on the flooding of the GDE during CO electrolysis cannot be assessed at present. Future investigations should monitor the differential pressure across the GDE during CO electrolysis to better understand the influence of a possible non-uniform pressure distribution. The contribution of electrowetting, on the other hand, could be investigated, for example, by incorporating more dielectric material (such as PTFE) into the GDE, which should suppress electrowetting during CO electrolysis[10].

Conclusions

The influence of the precipitation of the (bi)carbonate salt on the GDE flooding process was investigated with the developed operando water trap system. CO_2 electrolysis in $KHCO_3$- or

K_2CO_3-based electrolytes showed higher leakage rates and a faster shift to HER compared to KOH-based electrolytes. This indicates that the GDE flooding process was indeed enhanced by the faster formation of (bi)carbonate salt in the GDEs. Furthermore, when the pH of the 1 M KOH electrolyte was analyzed over time, it was found that the leakage from the GDE increased when the bicarbonate anion became the dominant species in the electrolyte. This indicates that $KHCO_3$ salt precipitation in particular accelerates the flooding of the GDE. IR experiments supported this hypothesis, as the formation of $KHCO_3$ in the GDE was confirmed even at a highly alkaline pH of the catholyte. In extension, the GDE flooding process during CO electrolysis was examined, where no $KHCO_3$ salt precipitation occurs. During CO electrolysis complete flooding was at least strongly suppressed and could no longer be quantified with the operando water trap. This is consistent with previous results, where bicarbonate formation and the resulting $KHCO_3$ salt precipitation was identified as the main cause of GDE flooding. However, the EDX and ICP-OES results showed that partial flooding of the catalyst layer also occurred during CO electrolysis, but at a slower rate. Despite the suppressed GDE flooding, CO electrolysis showed a faster shift towards HER. This could be due to the lower solubility of CO compared to CO_2 in aqueous electrolysis, which leads to a stronger limitation in mass transport during flooding. Overall, the present study shows that bicarbonate salt precipitation is one of the main reasons for GDE flooding during CO_2 electrolysis. Future studies to enhance the lifetime of CO_2 electrolysis should therefore focus on the suppression of salt formation in the GDE. It is important to mention that GDE flooding still occurs even when salt precipitation is avoided. Possible contributing factors, such as electrowetting or non-uniform pressure distribution in the GDE, also require future long-term investigations to overcome the limitations of stability for technical applications.

References

1. T. M. L. Wigley, *Climatic Change,* **5**(4), 315–320 (1983).
2. C. A. R. Pappijn, M. Ruitenbeek, M.-F. Reyniers and K. M. van Geem, *Front. Energy Res.,* **8,** 557466 (2020).
3. R. Sharifian, R. M. Wagterveld, I. A. Digdaya, C. Xiang and D. A. Vermaas, *Energy Environ. Sci.,* **14**(2), 781–814 (2021).
4. B. Belsa, L. Xia and F. P. García de Arquer, *ACS energy letters,* **9**(9), 4293–4305 (2024).
5. Y. Cheng, P. Hou, X. Wang and P. Kang, *Accounts of chemical research,* **55**(3), 231–240 (2022).
6. Y. Xie and Y. Wang, *Joule,* **8**(4), 879–881 (2024).
7. I. E. L. Stephens, K. Chan, A. Bagger, S. W. Boettcher, J. Bonin, E. Boutin, A. Buckley, R. Buonsanti, E. Cave, X. Chang, S. W. Chee, A. H. M. Da Silva, P. de Luna, O. Einsle, B. Endrődi, M. E. Escribano, J. V. Ferreira de Araujo, M. C. Figueiredo, C. Hahn, K. U.

Hansen, S. Haussener, S. Hunegnaw, Z. Huo, Y. J. Hwang, C. Janáky, B. S. Jayathilake, F. Jiao, Z. P. Jovanov, P. Karimi, M. T. M. Koper, K. Kuhl, W. H. Lee, Z. Liang, X. Liu, S. Ma, M. Ma, H.-S. Oh, M. Robert, B. R. Cuenya, J. Rossmeisl, C. Roy, M. P. Ryan, E. H. Sargent, P. Sebastián-Pascual, B. Seger, L. Steier, P. Strasser, A. S. Varela, R. E. Vos, X. Wang, B. Xu, H. Yadegari and Y. Zhou, *J. Phys. Energy (*2022).
8. M. H. Barecka, J. W. Ager and A. A. Lapkin, *STAR protocols,* **2**(4), 100889 (2021).
9. S. Hernandez-Aldave and E. Andreoli, *Catalysts,* **10**(6), 713 (2020).
10. M. Li, M. N. Idros, Y. Wu, T. Burdyny, S. Garg, X. S. Zhao, G. Wang and T. E. Rufford, *J. Mater. Chem. A,* **9**(35), 19369–19409 (2021).
11. C.-T. Dinh, T. Burdyny, M. G. Kibria, A. Seifitokaldani, C. M. Gabardo, F. P. García de Arquer, A. Kiani, J. P. Edwards, P. de Luna, O. S. Bushuyev, C. Zou, R. Quintero-Bermudez, Y. Pang, D. Sinton and E. H. Sargent, *Science (New York, N.Y.),* **360**(6390), 783–787 (2018).
12. D. Ren, J. Gao, S. M. Zakeeruddin and M. Grätzel, *J. Phys. Chem. Lett.,* **12**(31), 7583–7589 (2021).
13. M. W. Schreiber, *Current Opinion in Electrochemistry,* **44,** 101438 (2024).
14. F. Bienen, J. Hildebrand, D. Kopljar, N. Wagner, E. Klemm and K. A. Friedrich, *Chemie Ingenieur Technik,* **93**(6), 1015–1019 (2021).
15. L. M. Baumgartner, A. Goryachev, C. I. Koopman, D. Franzen, B. Ellendorff, T. Turek and D. A. Vermaas, *Energy Adv. (*2023).
16. R. Haaring, P. W. Kang, J. W. Lee, J. Lee and H. Lee, *ACS applied materials & interfaces,* **16**(22), 28731–28741 (2024).
17. J. Osiewacz, M. Löffelholz, B. Ellendorff and T. Turek, *Journal of Power Sources,* **603,** 234430 (2024).
18. C. P. O'Brien, D. McLaughlin, T. Böhm, Y. C. Xiao, J. P. Edwards, C. M. Gabardo, M. Bierling, J. Wicks, A. Sedighian Rasouli, J. Abed, D. Young, C.-T. Dinh, E. H. Sargent, S. Thiele and D. Sinton, *Joule,* **8**(10), 2903–2919 (2024).
19. Y. Xu, J. P. Edwards, S. Liu, R. K. Miao, J. E. Huang, C. M. Gabardo, C. P. O'Brien, J. Li, E. H. Sargent and D. Sinton, *ACS Energy Lett.,* **6**(2), 809–815 (2021).
20. Y. Kong, H. Hu, M. Liu, Y. Hou, V. Kolivoška, S. Vesztergom and P. Broekmann, *Journal of Catalysis,* **408,** 1–8 (2022).
21. E. R. Cofell, U. O. Nwabara, S. S. Bhargava, D. E. Henckel and P. J. A. Kenis, *ACS applied materials & interfaces,* **13**(13), 15132–15142 (2021).
22. J. Disch, L. Bohn, S. Koch, M. Schulz, Y. Han, A. Tengattini, L. Helfen, M. Breitwieser and S. Vierrath, *Nature communications,* **13**(1), 6099 (2022).
23. B. Sahin, M. Kraehling, V. Facci Allegrini, J. Leung, K. Wiesner-Fleischer, E. Magori, R. Pastusiak, A. Tawil, T. Hodges, E. Brooke, E. C. Corbos, M. Fleischer, E. Simon and O. Hinrichsen, *Journal of CO2 Utilization,* **82,** 102766 (2024).
24. M. Wrobel, S. Kriescher, T. Schiffer, R. Keller and M. Wessling, *Chemical Engineering Journal,* **474,** 145335 (2023).
25. B. de Mot, J. Hereijgers, M. Duarte and T. Breugelmans, *Chemical Engineering Journal,* **378,** 122224 (2019).
26. B. Sahin, S. Kimberly Raymond, F. Ntourmas, R. Pastusiak, K. Wiesner-Fleischer, M. Fleischer, E. Simon and O. Hinrichsen, *ACS applied materials & interfaces,* **15**(39), 45844–45854 (2023).
27. U. O. Nwabara, E. R. Cofell, S. Verma, E. Negro and P. J. A. Kenis, *ChemSusChem,* **13**(5), 855–875 (2020).
28. A. A. Samu, A. Kormányos, E. Kecsenovity, N. Szilágyi, B. Endrődi and C. Janáky, *ACS energy letters,* **7**(5), 1859–1861 (2022).
29. J. E. Huang, F. Li, A. Ozden, A. Sedighian Rasouli, F. P. García de Arquer, S. Liu, S. Zhang, M. Luo, X. Wang, Y. Lum, Y. Xu, K. Bertens, R. K. Miao, C.-T. Dinh, D. Sinton and E. H. Sargent, *Science (New York, N.Y.),* **372**(6546), 1074–1078 (2021).
30. J. Feng, L. Wu, X. Song, L. Zhang, S. Jia, X. Ma, X. Tan, X. Kang, Q. Zhu, X. Sun and B. Han, *Nature communications,* **15**(1), 4821 (2024).
31. D. Wu, F. Jiao and Q. Lu, *ACS Catal.,* **12**(20), 12993–13020 (2022).

32. D. M. Rottmann, R. Kollmuss, S. Haufe and K. J. J. Mayrhofer, *J. Electrochem. Soc. (*2025).
33. H. Zhang, J. Li, M.-J. Cheng and Q. Lu, *ACS Catal.,* **9**(1), 49–65 (2019).
34. J. Zosel, W. Oelßner, M. Decker, G. Gerlach and U. Guth, *Meas. Sci. Technol.,* **22**(7), 72001 (2011).
35. Z. Zhu, K. Z. Çolakhasanoğlu, R. L. E. G. Aspers, J. Meurs, S. M. Cristescu, T. Burdyny and E. W. Zhao, *ACS catalysis,* **15**(14), 12300–12307 (2025).
36. M. E. Leonard, L. E. Clarke, A. Forner-Cuenca, S. M. Brown and F. R. Brushett, *ChemSusChem,* **13**(2), 400–411 (2020).
37. J. Huang, N. Hörmann, E. Oveisi, A. Loiudice, G. L. de Gregorio, O. Andreussi, N. Marzari and R. Buonsanti, *Nature communications,* **9**(1), 3117 (2018).
38. J. Vavra, T.-H. Shen, D. Stoian, V. Tileli and R. Buonsanti, *Angewandte Chemie (International ed. in English),* **60**(3), 1347–1354 (2021).
39. M. Jouny, G. S. Hutchings and F. Jiao, *Nat Catal,* **2**(12), 1062–1070 (2019).
40. M. Jouny, W. Luc and F. Jiao, *Nat Catal,* **1**(10), 748–755 (2018).
41. L. Han, W. Zhou and C. Xiang, *ACS Energy Lett.,* **3**(4), 855–860 (2018).
42. T. Zhang, Z. Li, X. Lyu, J. Raj, G. Zhang, H. Kim, X. Wang, S. Chae, L. Lemen, V. N. Shanov and J. Wu, *J. Electrochem. Soc.,* **169**(10), 104506 (2022).
43. Y. Huang, A. D. Handoko, P. Hirunsit and B. S. Yeo, *ACS Catal.,* **7**(3), 1749–1756 (2017).